AUTOMATIC SHADOW DETECTION FOR HIGH-RESOLUTION REMOTE SENSING DATA

D. Prabhakar*, P.K Garg

Department of Civil Engineering, Indian Institute of Technology, Roorkee, India
(dprabhakar, p.garg)@ce.iitr.ac.in

Commission IV, WG IV/9

KEY WORDS: Shadow Detection, Shadow Masking, Image Processing, Thresholding, Color Space

ABSTRACT:

Shadow can be casted by daylight or any other light sources. We will not get a clear and quality image if it's hovered by the shadow. Shadows are frequently formed in high-resolution satellite imagery by the limitations of the imaging environment and the presence of high rise structures, and this scenario is true especially in metropolitan regions. Shadow is one of the noteworthy evils in remotely sensed imagery which hinders the precision of information extraction and change identification. To attenuate the effects of shadow in high resolution imagery regarding their supplemental functions, our paper suggests a novel algorithm for shadow masking built on computational methods. Firstly we transformed the images from RGB space to CIELCh space model, next we evaluated a modified Specthem ratio, and then used multilevel thresholding. We also created shadow masks for areas having vegetation, water, and soil. Shadow mask noise was decreased by morphological techniques. The ratio of lighting for the shadowed and unshadowed areas is utilized to create shadow masks, which are then used to remove shadows from the source photos. The thresholding approach creates an initial shadow mask during the shadow detection step, and the morphological filtering method is used to remove the noise and incorrect shadow regions. We also vectorized the raster data which can be further applied for various other studies.

1. INTRODUCTION

Added intricate information on land coverings (e.g., towers , high rise structures, farmlands, bridges, roads, vegetation, etc) can be secured effortlessly from high-spatial-resolution (H S R) multispectral satellite remote sensing illustrations which the HSR satellites capture (such as GeoEye-1, IKONOS, WorldView-2, WorldView-3, QuickBird, etc.) (Finlayson et al. 2006, Tian et al. 2016, Kang et al. 2017, Schläpfer et al. 2018, Zhao et al. 2015). Change detection, object recognition, and picture categorization are a few applications of HSR images that can be used, however, the shadows cast by land objects and clouds are unavoidable and have a more significant impact. High-resolution remote sensing has become increasingly popular and dominant in urban remote sensing during the past ten years (Rashed and Jürgens, 2010, Weng and Quattrochi 2018). However, shadows have a significant negative impact on medium and high-resolution remote sensing photos, especially in urban regions with plenty of tall structures, which causes considerable information loss for those images (Luo et al. 2015). In addition to being used for the three-dimensional reconstruction of structures, accurate shadow extraction and information restoring in shadow areas also have significant applications in the classification of urban features, urban planning, road network extraction, impervious layer research, (Lorenzi et al. 2012, Zhou et al. 2009, Sabri et al. 2019), etc.

Colour tone is a potent descriptor in colour remote sensing images that not only streamlines and controls the distinguishing qualities of visual interpretation applications. Mankind describes a body's colour in terms of hue, saturation, and brightness characteristics, which are specified by a number of related colour models like and CPU-intensive to the point of being ineffective for real-time image processing. HSV, HSL, and HIS (hue saturation intensity / value). Numerous writers have provided multiple equations for the same colour space as a result of the abundance of distinct HSL class colour spaces in the resources and their machine dependencies. Even though they are excellent for user interfaces, particularly colour choice, those HSL-related colour spaces only approximate the illumination information in the image and sometimes confuse hue and lightness or saturation with it. A suitable colour space, such as the CIELAB-designed CIEL * a * b * (CIELAB) or its polar equivalent CIELCh, is necessary for accurate lightness calculations (CIE). This colour space describes all observable hues mathematically in 3 dimensions: ‘L’ is for lightness and ‘a’ and ‘b’ for the complementary hues of green - red and blue - yellow. The module is C in CIELCh, and the angle of the [a, b] coordinate is ‘h’. Boundary ambiguity, colour variations, different lighting conditions, weather effects, and other issues might make it difficult to distinguish between shadows. It has been observed that shadowed regions in color multispectral images hold the following properties:-

- Lower brightness (intensity) as a result of the sun's electromagnetic energy being obstructed (Tsai, 2006).
- Greater saturation with shorter blue - violet wavelengths as a result of air scattering's Rayleigh effect (Polidorio et al., 2003).
- Higher values of hue due to the wavelength-dependent strength shift in the shaded area compared to an unlit area (Huang et al., 2004).
- A rise in entropy, a measure of the randomness of the pixels there (Zhu et al., 2010).

*Corresponding author

In recent decades, a significant study has been performed on the identification of shadows in both multispectral satellite remotely perceived photos along with colour airborne imagery. A shadow identification technique was put out by (Huang et al. 2004) by creating an image model that showed that shadow regions had more hue values than the matching non-shadow unities. After the specific threshold was adopted to get the shadow entrant in agreement with the higher values of hue in shadow zones, 2 further thresholds were utilised in regards to the bluish and greenish elements to enhance the shadow intrant by removing the green and blue non-shadow items. The deduced shadow identification technique was initially focused on determining the blue and green non-shadow entity misclassification error in colour airborne photographs, despite the fact that thresholds were manually chosen. Huang et al. constructed a good imaging model despite the manual threshold selection. The shadow identification results of the two multispectral images, QuickBird and IKONOS, across the C1, C2, and C3 modules of the colour spaces C1C2C3, correspondingly, were also examined by (Sarabandi et al. 2004), who then proposed a C3 shadow detection approach. The C3-based method is capable of detecting the broad outline of significant shadow patches. However, the bulk of greenish nonshadow objects were mislabeled. Similar to this, Arevalo et al. (2006) created a region growing technique for High spatial resolution pan sharpening satellite remote sensing images and a semi automatic shadow recognition system based on the 'C3' section of C1-C2-C3 colour spaces.

Comparative tests showed that the proposed shadow detection method outperformed the algorithms based on the R-G-B model by (Huang et al. 2004) and the 'C3' model by (Sarabandi et al. 2004) in terms of accuracy and resilience. (Besheer et al.2015) suggested a modified-C3 (M C 3) index by establishing an enhanced C1-C2-C3 invariant colour spaces using near infrared (NIR) band evidence in supplement to observable bands (i.e. red, green, and blue bands) in the actual C1-C2-C3 constant colour spaces, taking into account all available bands of the multispectral image. Following that, a bimodal histogram threshold was used to segment the shadow. Compared to the C3 approach developed by (Sarabandi et al. 2004) and (Arevalo et al. 2006), the performance of the MC3 method was enhanced by taking the NIR component into account.

Additionally, (Silva, et at. 2018, and Tsai 2006) produced an automatic shadow identification method that was property based and which used the ratio of hue upon intensity values, known as the spectral ratio index (SRI) shadow detection method, based on the Huang's imaging model (Huang et al. 2004) and the Phong lighting model (Phong 1975). An ideal threshold was then picked up automatically using the Otsu thresholding method (Otsu 1979). The SRI algorithm was evaluated by comparative experiments using colour aerial photos in the HIS, HSV, HCV, YIQ, and YCbCr invariant colour spaces. In HIS, YIQ, and YCbCr colour spaces, the comparison results demonstrated that the SRI shadow detection method produced greater shadow identification precisions, albeit some green grass in non-shadow areas were yet space (e.g., histogram equalization and box filter). Studies somewhat misclassified. After that, (Khekade et al. 2015) used a number of post-processing techniques to improve the shadow detection outcomes of Tsai's SRI algorithm; particularly in the YIQ invariant colour comparing colour aerial photographs to Tsai's original SRI images revealed that the upgraded shadow-detection method significantly reduced the shadow lapse issue from a pictorial perspective. (Chung et al. 2009) offered a modified ratio map based on Tsai's effective shadow detection technique, employing an exponent function for the SRI developed by Tsai, and presenting a successive thresholding strategy (STS) as opposed to just utilizing a global threshold. The suggested approach by (Chung et al. 2009) demonstrated increased performance in recognizing shadow in photos comprising lower brightness entities, according to experiments done on coloured aerial photographs. Inspired by (Chung et. al's 2009) STS method. The logarithmic spectral ratio index (LSRI) algorithm was created by (Silva et al.2017) to improve the SRI approach of (Tsai 2006) exclusively in the CIELCh colour spaces by employing a natural log function to the initial ratio map to condense the initial outputs. Multilevel thresholding was then used to segment the ratio map. By correctly identifying shadows and preventing the misclassification of dark areas, this modified ratio technique outperformed the initial method of ratio by (Tsai , 2006) and the method of STS by (Chung et al. 2009) in colour aerial photos. A comparable shadow detection technique was also published by (Ma et al. 2008) using the HSV colour space's normalized saturation-value index (NSVDI). The NSVDI technique was initially used to create a crude shadow-index view. The ultimate shadow view with a certain threshold was then created by segmenting the rough shadow index image. Despite leaving out some small shadow, this NSVDI approach did a good job of detecting large shadow in IKONOS multispectral photos. A shadow detector index (SDI) was also presented for the purpose of detecting shadows in HSR multi-spectral satellite remote-sensing imageries. The neighbourhood valley-emphasis method (NVEM) was used to binarise the SDI index image to obtain the image of shadow after first analyzing the differences between typical non-shadow and shadow, specifically for vegetation, in relation to blue and green elements. With the exception of a few minor hiccups, the SDI technique achieved excellent shadow detection accuracies and functioned well in differentiating shadow from vegetation. Although more and more shadow detection algorithms have been proposed in recent years for detecting shadow in colour aerial images and HSR multispectral satellite remote sensing images, there are still issues that need to be resolved with regard to shadow detection, most notably high small shadow omission and typical non-shadow misclassification (like bluish and greenish dark non-shadow misclassification, as well as large dark non-shadow misclassification). As a result, shadow identification in HSR multispectral satellite remote sensing photos remains difficult.

In our work, we present our shadow detection process in depth, reviewing every stage to produce a final shadow mask, and then we explain our shadow elimination process.

2. SHADOW DETECTION APPROACH

The shadows appear in places where a source of light cannot directly reach because of an obstacle caused by another item. A shadow can be cast by an object itself. Shadow detection in this work is carried out in the LAB colour space. The RGB image is first transformed into its LAB equivalent, then into its polar representation, CIELCH. One of the approaches is then chosen for shadow detection based on the mean value of the image in the A and B planes. Finding characteristics of shadows is the basis for shadow detection. These characteristics are intended to distinguish shadows from the background and nearby objects.

The technique for identifying shadows used in this study expands on Silva and Tsai's approach, which makes use of colour spaces that

Figure 1. Original image acquired form Worldview-3 for Bangalore, India.

Sr. No	Steps
i	RGB conversion to CIELab
ii	Conversion to CIELCH
iii	Flattening out the L and h channels
iv	Segmenting the shadow using the Specthem ratio as a threshold
v	Multiple thresholding using K - Means clustering algorithm
vi	Shadow mask morphological erosion
vii	Noise reduction through dilation

Table 1. Shadow detection algorithm

Sr.no.	Steps
i	Decide how many clusters you want by entering the number K.
ii	Pick K centroids or random spots.
iii	Each data point should be assigned to its closest centroid, which will produce the K predetermined clusters.
iv	Based on the updated variance estimate, set a new centroid for each cluster.
v	Repetition of the third step is necessary to reassign every data point to the new centroid of each cluster.
vi	If there has been a reassignment, move on to step 4; if not, go to FINISH.
vii	Now, the model is finished.

Table 2. K Means Clustering Algorithm

Sr. No	Steps
i	Mask should be divided into designated, connected areas.
ii	Obtain the shaded region using subMask.
iii	Take the subMask out of the dilated subMask.
iv	Use borderMask to get unshaded borders.
v	Calculate the ratio of illumination between the border and the shadow area.
vi	Based on Ratio, relight the pixels.
vii	Return Enhanced

Table 3. Shadow removal algorithm

separate light and chromaticity information (Tsai, 2006, Silva et al.2018). In our method, the updated Specthem Ratio image was segmented using multilayer global thresholding. This was motivated by (Chung et al's 2009) successive local thresholding proposal. In addition, in our study the multilevel Otsu thresholding method is not used in view of the computational complexity and time cost incurred. As such, it is replaced by the K - Means clustering algorithm, which is another method to determine the multiple thresholds in a global context, which would give a close approximation to that of the multilevel Otsu thresholding method. Consequently, our suggested strategy adopts these stages. (Table 1):

(a) Converting an image from the RGB model to the CIELAB model to segregate the data about colour and intensity.
(b) Conversion of the CIELAB colour space to its polar equivalent, CIELCh, allowing us to take use of the hue channel's greater hue values in shadows.
(c) Image noise reduction by smoothing the L channel and h channel.
(d) Using CIELCh instead of HSI colour space in the modified specthem ratio computation of $\frac{h+1}{L+1}$.
(e) Shadow segmentation applying the higher threshold discovered by the multi-level application of the K-Means clustering algorithm of thresholding on the spectrum ratio image.
(f) Morphologically eroding the shadow mask, and then dilating to reduce noises and improve shadow region delineation.

2.1. Image transformation from RGB-space to CIELCh-space

The RGB colour space used by colour multispectral images is converted to the CIELCh colour spaces, which is a polar form of the CIELAB colour spaces created by the Commission Internationale de l'Éclairage (CIE) to simulate how people see colour. As long as there is enough light, we see colour as being roughly constant regardless of the illuminant.

The CIE tri-stimulus CIEXYZ is used to calculate the device-independent CIELAB colour space. This colour space is not very obvious, regardless of the channel L getting a decent association with observed lightness (Ford and Roberts, 1998). In contrast, it's polar twin, the CIELCh space, uses illumination, chroma, and hue to define colours.

In order to specify all visible colours using only positive values, the CIEXYZ colour space must first be converted from RGB to that format (Ford and Roberts, 1998). For the conventional 2º observer and D-65 illuminant, this transformation is represented by

$$\begin{bmatrix} X \\ Y \\ Z \end{bmatrix} = \begin{bmatrix} 0.4124564 & 0.3575761 & 0.1804375 \\ 0.2126729 & 0.7151522 & 0.0721750 \\ 0.0193339 & 0.1191920 & 0.9503041 \end{bmatrix} \begin{bmatrix} R \\ G \\ B \end{bmatrix} \quad (1)$$

where the International Commission of Illumination (CIE) defined the "2o standard observer" as the typical human's chromatic reaction within a 2o arc inside the fovea. The CIE also specifies D65 as a standard illuminant that is often used. It is also known as a daylight illuminant because it roughly reflects the typical midday light in Western and Northern Europe (which is made up of both the light from the sun and the light reflected off of a clear sky).

We derive the L, a, and b channels from the XYZ tri-stimulus in the manner shown below. (Ford and Roberts, 1998)

$$L = \begin{cases} 116 \left(\frac{Y}{Yn}\right)^{\frac{1}{3}} - 16 & if \frac{Y}{Yn} > 0.008856 \\ 903.3 \left(\frac{Y}{Yn}\right) & if \frac{Y}{Yn} \leq 0.008856 \end{cases} \quad (2)$$

$$a = 500 \left(f\left(\frac{X}{Xn}\right) - f\left(\frac{Y}{Yn}\right) \right) \quad (3)$$

$$b = 200 \left(f\left(\frac{Y}{Yn}\right) - f\left(\frac{Z}{Zn}\right) \right) \quad (4)$$

where

$$f(x) = \begin{cases} x^{1/3}, & if x > 0.008856 \\ 7.787 + \frac{16}{116}, & if\ x \leq 0.008856 \end{cases} \quad (5)$$

The terms Xn, Yn, and Zn in the equations above relate to the referenced white, which has the values XYZ = {95.047, 100.00, 108.883} for D65 illuminant with Y = 100.

Simple geometric transformation can convert the CIELAB colour system's cartesian coordinates into the CIELCh colour space.

$$C = \sqrt{a^2 + b^2} \quad (6)$$

h=atan2 (b,a)

$$h = \begin{cases} h + 360° & if\ h < 0° \\ h - 360° & if\ h \geq 360° \end{cases} \quad (7)$$

where atan2 is a particular function found in several standard libraries that explains what happens when a = 0.

2.2. Specthem ratio

We determined the ratio between the hue and intensity values of the pixels throughout the picture segmentation process to produce shadows. Instead of the channels H and I from HSI suggested by Tsai (2006), we used the channels L and h from the CIELCh space. Thus, our modified Specthem ratio is:

$$S_r = \frac{(h+1)}{(L-1)} \quad (8)$$

where Sr is the image of the Specthem ratio, and the channels h and L have in the past been normalised to the [0,1] interval.

The original image's hue to intensity ratio will draw attention to the heightened hue attribute of shadows with low luminance (intensity), meaning that the pixels in shaded areas will have greater values than those in unshaded areas.

2.3. K-Means Clustering Algorithm

To handle clustering issues in data science or machine learning, K-Means Clustering which is an unsupervised learning algorithm process is used that divides the unlabeled information into various clusters. Here, K specifies how many pre-defined clusters must be produced during the operation.

It gives us the ability to divide the data into various groups and provides a practical method for automatically identifying the algorithm is centroid-based. Reducing the overall distances between each data point and its matching clusters is the main objective of this technique. An unlabeled dataset is first used as the algorithm's input, after which it is divided into k clusters. The algorithm then repeats this process until it has no more clusters left to use. K should be set to a predetermined value for this method.

The two major functions of the k-means clustering algorithm are:

- Uses an iterative technique to choose the best value for K centre points or centroids.
- Places every data point with the nearest k-center. A cluster is formed by the data points that are close to a specific k-center.

As a result, each cluster is distant from the others and contains data points with some commonality. The K-means Clustering Algorithm (Table 2) is explained in Fig. 2.

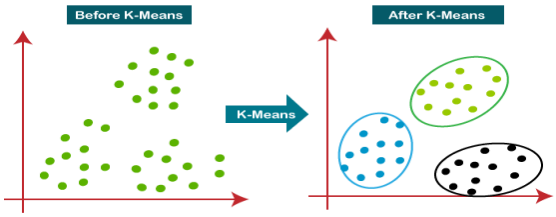

Figure 2. K Means Clustering Algorithm

2.4. Operations for morphology and noise reduction

Often, thresholding results in some noise in the form of loose pixels in the segmented images. Given that the image is binary, one way to eliminate those pixels is to use morphological operations like Opening and Closing (Gonzalez and Woods, 1992).

To remove noise and properly integrate boundaries (penumbra) in the shadow mask that has been segmented from the Specthem ratio, we perform morphological Closing.

Closing operations are described as the enlargement of the image A by the structuring element B and the subsequent erosion of the clusters in the unlabeled dataset without the requirement for any training. Each cluster has a centroid assigned to it because the outcome by B. Although it also removes holes, closing tends to smooth the edges of the object.

3. SHADOW REMOVAL APPROACH

Each pixel in the binary mask created by the shadow detection method is roughly categorised as either being in a shadow or not. However, the penumbra region in an actual scene causes a gradual change in illumination, which needs to be taken into account. Calculations for an image with shadows include (Table 3):

$$I_i = (k_i L_d + L_e) R_i \quad (9)$$

where Ii is the pixel value for the image with the shadow, Ld is the direct light intensity, and Le is the environmental light intensity. The reflectance of the pixel is represented by Ri, while its shadow status is represented by ki.

Assuming that direct light strikes each pixel at the same angle, we can assume that each pixel is illuminated uniformly. In Eq. (9), if ki is 0, the pixel is in an umbra because it receives no artificial illumination; if ki is 1, the pixel is in a nonshadow region. Our shadow detection technique yields a hard shadow map with ki being either 1 or 0.

Our shadow removal approach was created to be suitable for parallel computation and is an adaption of the work by Silva G.F.2018, Guo et al. (2013), and Ye et al. (2012). It is composed by:

i. Marking shaded areas' connected components in virtue to make separate submasks for every shaded area's corresponding local handling.
ii. Estimating the lighting ratio of the shadow areas and their borders in order to determine the co-efficient required to make up for the absence of direct illumination in shaded areas
iii. Relighting the shaded areas by multiplying pixels in accordance with the shadow mask and the region illumination ratio.
iv. Compensation of Penumbra .

Figure 3. Generated Shadow mask of the study are

Figure 4. De-shadowed Image.

4. RESULTS AND DISCUSSION

The original image that was used to gauge how well each implementation performed is shown in Fig. 1. To test the algorithms of our detection technique, it is equivalent to the input colour multispectral image obtained from urban regions. Fig. 3 depicts the shadow mask created from the source image. (Fig.1). We begin processing of the first Image by matching the multispectral imagery in RGB format (Fig. 1) to CIELCh spaces. The zones of lower luminance are emphasized after using the Specthem ratio. The final mask is obtained after morphological and thresholding processes. Fig. 3 shows the final mask. The retrieved shadow is shown as white pixels. Using the shadow mask, we then estimate the ratio of illumination between the (unshaded) boundaries and shaded area. Lastly, we regenerate the shaded pixels to provide the deshadowed image as shown in Fig. 4.
Figure 1 has good resolution and distinct shadows. The suggested method was capable to locate shadow patches in a grassy environment. Noise reduction deleted irrelevant dark areas. The masking technique still provides some challenges to the system, but it successfully differentiated the bottom tree from its shadow while accurately counteracting the shadows (Fig. 3). Some false positives are discovered, or some pixels are misclassified as shadow regions. Some building faces were recognised as shadows, causing false positives. In Fig. 4, most of the shadows in Fig. 3 have been eliminated, allowing us to identify the shaded objects. Even shadows were removed. We also observe that the buildings' non-illuminated faces were relit. The absence of tree shadows is the most crucial thing to notice. We can observe that the trees' appearance is unaltered despite the absence of shadows.

It can be seen that the Image 03 missed few shadows present in it. hat is brought on by the image's intricacy and low resolution. Due to the image's poor contrast, cast shadows (buildings without lights on their faces) and cast shadows (buildings casting shadows on a road) frequently overlap. The improved noise immunity of our suggested strategy led to greater performance.

Using the CUDA Python code, we can see that each image's processing of shadow detection takes a longer amount of time. This results from the fact that memory transfers between the CPU and GPU, which are the primary bottlenecks in GPU programming. CUDA boosts performance even further when there are more calculations than shadow since the speed improvements outweigh the disadvantage of memory transfers.

Shadow segmentation is not the only processing step taken into account when comparing sequential versus parallel solutions. Parallel implementations of stages like colour conversion, Specthem Ratio calculation, and morphological operations contribute to the increase in computational speed.

5. CONCLUSION

We used a high resolution remote sensing image of a real scene, obtained through high resolution remote sensing image, with scene complexities. We initiated by mapping the RGB-formatted multispectral images into CIELCh space. The low luminance areas were then highlighted in the Specthem Ratio images that we had generated earlier. To acquire raw masks, we then conducted multilayer thresholding. The final shadow masks were then created by applying morphology techniques, which preserved the shapes of the masks and reduced noise. After that, we applied the masks to carry out local processing in the shadowy areas. To relight the shaded pixels, we used the statistical data of their bounds, which were not shaded, to relight the boundaries.

The strengths of each technique described in Silva et al. (2018), Chung et al. (2009), and Tai (2006) were examined in this work. Multilevel thresholding procedures and morphology were used to cover the brightness and chromaticity characteristics of the shadows. These procedures do away with the requirement for a priori knowledge of the surroundings, geometry, and location of the light source in order to reconstruct a 3D model, which can be time-

Figure 5. Vectorized image of the study area.

and CPU-intensive to the point of being ineffective for real-time image processing.

One can observe how the shadows are correctly detected in our suggested method, but dark parts that are not shadows are only marginally identified. It should be noted that false positives, or pixels that are mistakenly classified as shadows when they are not, have little impact in this type of image application. False negatives or unnoticed shadows would be the most dangerous scenario, which our strategy helps to reduce. To cut down on false positives, extra work on the thresholding technique might be required for some applications.

When comparing GPU implementation with CPU implementation, we found speedups of about 6 times. This increase in processing speed demonstrates the method's potential for application in a real-time monitoring system to boost the effectiveness of other algorithms. We also vectorized for further analysis (Fig 5)

6. ACKNOWLEDGEMENT

We appreciate the reviewers' insights and helpful criticism, which allowed us to make the paper better and Indian Institute of Technology Roorkee for providing us the funds.

REFERENCES

Arevalo, V.; González, J.; Valdes, J.; Ambrosio, G. Dectecting shadows in Quickbird satellite images. In Proceedings of the ISPRS Commission VII Mid-term Symposium “Remote Sensing: From Pixels to Processes”, Enschede, The Netherlands, 8–11 May 2006.

Besheer, M.; Abdelhafiz, A. Modified invariant color model for shadow detection. Int. J. Remote Sens. **2015**, 36, 6214–6223.

Chung, K.-L.; Lin, Y.R.; Huang, Y.H. E_cient shadow detection of color aerial images based on successive thresholding scheme. IEEE Trans. Geosci. Remote Sens. **2009**, 47, 671–681.

Finlayson, G. D., Hordley, S. D., Lu, C., & Drew, M. S. (2005). On the removal of shadows from images. *IEEE transactions on pattern analysis and machine intelligence*, *28*(1), 59-68.

Ford, A., & Roberts, A. (1998). Colour space conversions. *Westminster University, London*, *1998*, 1-31.

Gonzalez, R. C., & Woods, R. E. (1992). Digital image processing addison-wesley. *Reading, Ma*.

Guo, R., Dai, Q., & Hoiem, D. (2012). Paired regions for shadow detection and removal. *IEEE transactions on pattern analysis and machine intelligence*, *35*(12), 2956-2967.

Huang, J.J.; Xie,W.X.; Tang, L. Detection of and compensation for shadows in colored urban aerial images. In Proceedings of the 5th World Congress on Intelligent Control and Automation, Hangzhou, China,
15–19 June 2004.

Kang, X., Huang, Y., Li, S., Lin, H., & Benediktsson, J. A. (2017). Extended random walker for shadow detection in very high resolution remote sensing images. *IEEE Transactions on Geoscience and Remote Sensing*, *56*(2), 867-876.

Khekade, A.; Bhoyar, K. Shadow detection based on RGB and YIQ color models in color aerial images. In Proceedings of the 1st International Conference on Futuristic Trend in Computational Analysis and Knowledge Management (ABLAZE 2015), Greater Noida, India, 25–27 February 2015.

Lorenzi, L., Melgani, F., & Mercier, G. (2012). A complete processing chain for shadow detection and reconstruction in VHR images. *IEEE transactions on geoscience and remote sensing*, *50*(9), 3440-3452.

Luo, H., Wang, L., Shao, Z., & Li, D. (2015). Development of a multi-scale object-based shadow detection method for high spatial resolution image. *Remote Sensing Letters*, *6*(1), 59-68.

Ma, H.J.; Qin, Q.M.; Shen, X.Y. Shadow segmentation and compensation in high resolution satellite images. In Proceedings of the IEEE International Geoscience and Remote Sensing Symposium (IGARSS 2008), Boston, MA, USA, 7–11 July 2008.

Otsu, N. A threshold selection method from gray level histograms. IEEE Trans. Syst. Man Cybern. **1979**, 9,
62–66.

Phong, B.T. Illumination for computer generated pictures. Graph. Image Process. **1975**, 18, 311–317 Rashed, T., & Jürgens, C. (Eds.). (2010). *Remote sensing of urban and suburban areas* (Vol. 10). Springer Science & Business Media.

Sabri, M. A., Aqel, S., & Aarab, A. (2019). A multiscale based approach for automatic shadow detection and removal in natural images. *Multimedia Tools and Applications*, *78*(9), 11263-11275.

Sarabandi, P.; Yamazaki, F.; Matsuoka, M.; Kiremidjian, A. Shadow detection and radiometric restoration in satellite high resolution images. In Proceedings of the 2004 IEEE International Geoscience and Remote Sensing Symposium, Anchorage, AK, USA, 20–24 September 2004.

Schläpfer, D., Hueni, A., & Richter, R. (2018). Cast shadow detection to quantify the aerosol optical thickness for atmospheric correction of high spatial resolution optical imagery. *Remote Sensing*, *10*(2), 200.

Silva, G.F.; Carneiro, G.B.; Doth, R.; Amaral, L.A.; Azevedo, D.F.G.d. Near real-time shadow detection and removal in aerial motion imagery application. J. Photogramm. Remote Sens. **2017**, 2017, 104–121.

Tian, J., Qi, X., Qu, L., & Tang, Y. (2016). New spectrum ratio properties and features for shadow detection. *Pattern Recognition*, *51*, 85-96.

Tsai, V.J.D. A comparative study on shadow compensation of color aerial images in invariant color models. IEEE Trans. Geosci. Remote Sens. **2006**, 44, 1661–1671.

Weng, Q., & Quattrochi, D. A. (2018). *Urban remote sensing*. CRC press. Ye, Q., Xie, H., & Xu, Q. (2012). Removing shadows from high-resolution urban aerial images based on color constancy. *ISPRS-International Archives of the Photogrammetry, Remote Sensing and Spatial Information Sciences*, *39*, 525-530.

Zhao, J., Zhong, Y., & Zhang, L. (2014). Detail-preserving smoothing classifier based on conditional random fields for high spatial resolution remote sensing imagery. *IEEE transactions on geoscience and remote sensing*, *53*(5), 2440-2452.

Zhou, W., Huang, G., Troy, A., & Cadenasso, M. L. (2009). Object-based land cover classification of shaded areas in high spatial resolution imagery of urban areas: A comparison study. *Remote Sensing of Environment*, *113*(8), 1769-17